

Size distribution of dry AOT aggregates in apolar solvent using free energy evaluation

Ryo Urano¹ and John E. Straub^{1, a)}

*Chemistry Department, Boston University, 590 Commonwealth Avenue, Boston,
MA 02215 USA*

(Dated: 2017/09/07)

Normal micelle aggregates of amphiphilic surfactant in aqueous solvent are formed by a process of entropically driven self-assembly. The self-assembly of reverse micelles from amphiphilic surfactant in non-polar solvent in the presence of water is considered to be an enthalpically driven process. While the formation of normal and reverse surfactant micelles has been well characterized in theory and experiment, the nature of “dry” micelle formation, from amphiphilic surfactant in non-polar solvent in the absence of water, is poorly understood. In this study, a theory of “dry” reverse micelle formation is developed. Variation in free energy during micelle assembly is derived for the specific case of AOT surfactant in isooctane solvent using atomistic molecular dynamics simulation analyzed using the energy representation method. The existence and thermodynamic stability of “dry” reverse micelles of limited size are confirmed. The finite size is a clear signature of a critical micelle concentration, commonly observed in the formation of normal surfactant micelles. The morphology of larger dry micelles provides insight into the nature of the thermodynamic driving forces stabilizing the formation of the surfactant aggregates. Overall, this study provides detailed insight into the structure and stability of dry reverse micelles assembly in non-polar solvent.

Keywords: reverse micelle, size distribution, energy representation, molecular dynamics

^{a)}corresponding author e-mail: straub@bu.edu ; R. Urano and J. E. Straub contributed equally to this work.

INTRODUCTION

The rich phase behavior and complex dynamics of microemulsions have been a focus of intense experimental, theoretical, and computational study for decades. The detailed dynamic and thermodynamic behavior of ternary mixtures of surfactant, oil, and water are fundamentally important to the theory of complex solutions. In addition, self-assembled structures such as micelles, reverse micelles, and membranes have great applied importance to biology, as well as environmental and industrial chemistry. As such, the development of a fundamental understanding of the equilibrium state of microemulsions has been a critical goal for the field.

A phase of particular interest is the microemulsion composed of reverse micelles (RMs) in which amphiphilic surfactant aggregates containing a water core are suspended in non-polar solvent. The RM morphology has been exploited for a variety of applications, including chemical synthesis¹, drug delivery systems²⁻⁴, studies of model membranes⁵, and solute encapsulation^{6,7}. While an empirical approach to the optimization of surfactant mixtures has led to significant advancement, it has proven difficult to physically characterize RM solutions in terms of the distribution of aggregate size and nature of RM structure. As such, there is a pressing need to develop a first-principles theory for the *de novo* prediction of the RM size distribution as a function of solution composition.

The assembly of normal surfactant micelle in water solvent has long been assumed to be driven by an increase in water entropy following surfactant aggregation and exclusion of water from the micelle interior, leading to favorable changes in entropy and enthalpy upon micelle assembly.⁸⁻¹⁴ The assembly of “wet” RMs from a ternary mixture of surfactant, oil solvent, and water is typically considered to be enthalpy driven, with the RM phase stabilized by favorable interaction of water and surfactant head groups¹⁵. In contrast, clear identification of the principal driving force underlying the formation of “dry” RMs from surfactant in oil solvent in the absence of water has remained elusive¹⁶. As such, the mechanism of surfactant aggregation in oil solvent in the absence of water, and the very existence of “dry” RMs continues to be debated.

In early theoretical work, Ruckenstein and Nagarajan¹⁷ used a free energy functional approach for AOT surfactant in non-polar solvent to argue that interaction between surfactant head groups and tails creates a free energy minimum associated with the stable formation

of “dry” reverse micelles. Stable “dry” RM aggregates were predicted to be restricted to a gradual increase in “aggregation number” (number of AOT surfactant molecules in a given micelle) of less than ten, suggesting the absence of a critical micelle concentration (CMC). Given this prediction, it has been suggested that the experimentally observed CMC in “dry” RM mixtures must result from the presence of trace water molecules (carried over from AOT synthesis and incomplete surfactant “drying”) in a ratio of less than one water per AOT molecule. Motivated by experiments¹⁸ suggesting an inverse hexagonal structure in pure sodium AOT solutions, Harrowell et. al.¹⁹ investigated the structure of dry reverse micelles in sodium-sulfate ion clusters in the vacuum state. Considering the observed sodium-sulfate ion cluster structure and the structure of wet AOT reverse micelles as a perturbation of the crystal structure, they obtained a mean aggregation number that was macroscopically large, suggesting that AOT is insoluble in oil solvent.

A variety of experimental studies have proved the existence of “dry” RMs. Calorimetric studies^{20–22} confirmed that the stabilizing interaction energy between AOT molecules in organic solvents is so low as to make the formation of AOT oligomers improbable. In contrast, studies based on neutron scattering²³ and absorption spectroscopy²⁴ support the existence of a critical micelle concentration. In addition, a variety of studies have led to independent assessments of mean aggregation numbers (N_0) for surfactants in non-polar solvents, including $N_0=18$ by vapor pressure²⁵, and $N_0=39$ and $N_0=56$ by light scattering^{26,27}. More recent small-angle neutron scattering studies^{28,29} have shown a sharp transition in the mean aggregation number as a function of AOT concentration in non-polar solvents. Taken together, these experimental studies provide clear support for the existence of a CMC related to “dry” RM formation at higher AOT concentrations. Interestingly, these studies also demonstrate that the AOT aggregate size distribution sensitively depends on solvent properties, such as dielectric constant and surfactant solubility³⁰.

Significant theoretical work has been done to define the size distribution of surfactant micelles in water solvent. Christopher and Oxtoby³¹ proposed a density functional model that assessed free energy contributions to the aggregation process, obtaining a size distribution from numerical minimization of the free energy. Mohan and Kopelevich³² obtained kinetic rate constant for formation of spherical micelles formed by non-ionic surfactants using a coarse grained model and kinetic analysis. Kindt³³ employed the chemical species model³⁴ and a statistical dynamical equation for the size distribution parameterized with

an equilibrium constant obtained from molecular simulation. Kinoshita and Sugai^{35,36} also employed the chemical species model but used the reference interaction site model (RISM) integral equation theory in their simulations to obtain the chemical potential for surfactant aggregates of varying size. In an impressive theoretical study of the equilibrium properties of micelle formation, Yoshii and Okazaki^{37–40} employed the chemical species model to obtain a thermodynamic relation defining micelle aggregation number in terms of the chemical potential difference between micelles of varying size and the surfactant activity coefficient. The chemical potential difference was evaluated using thermodynamic integration and molecular dynamics simulation, while the activity coefficient was extracted from experimental data fit to Debye-Huckel theory. The result was a *de novo* theoretical prediction of the CMC and distribution of micelle size as a function of surfactant concentration.

In this work, we extend the seminal work of Yoshii and Okazaki to the study of “dry” AOT reverse micelles. In order to address the inherent complexity of the reverse micelle system, chemical potential differences between surfactant aggregates of varying size are evaluated using the classical free energy functional based Energy Representation (ER) method^{41–43}. The ER method is shown to dramatically increase the efficiency of free energy calculation within sufficient accuracy to provide thermodynamically relevant results. The resulting theory provides a *de novo* prediction of the surfactant aggregate size distribution, providing evidence for the existence of stable dry AOT RMs and surprising insight into the RM structure and stability.

This paper is organized as follows. In the Methods section, we derive a thermodynamic relation for the relative stability of AOT aggregates as a function of aggregate number. The theoretical foundation for the evaluation of the chemical potential as a function of aggregate size based on free energy calculations is described in detail. In the Results section, we first determine the free energy of solvation for AOT surfactant in isooctane solvent in the energy representation method. Subsequently, the structures and relative free energies of dry AOT RMs are characterized as a function of aggregation number. The mean aggregation number is derived and interpreted in terms of size-dependent aggregate structural changes. Finally, the theoretical results are used to address discrepancies between prior theoretical predictions and experimental observations. Overall, this study provides the first detailed atomic-level characterization of the equilibrium distribution of dry AOT reverse micelles.

METHODS

Thermodynamic relation for size distribution of each composition

The theoretical foundation of our approach is a definition relating the relative concentration of a dry micelle of a given size to the free energy difference between micelles of varying size and the corresponding activity coefficient. The starting point is the previous works of Okazaki and coworkers exploring the thermodynamic properties of surfactant micelles^{37–40}.

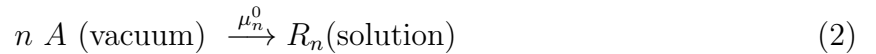
The chemical species model is employed^{31,33,35,44–46} in which the composition of the solution is defined in terms of a distribution of RMs of varying size assuming that each aggregate (and the monomer as well) is considered to be a distinct species.

The chemical potential μ_n of a reverse micelle composed of n amphiphilic surfactant molecules, A , is written

$$\mu_n = \mu_n^0 + k_B T \ln a_n \quad (1)$$

where μ_n^0 is the standard state chemical potential of an isolated micelle R_n of aggregation number n , and a_n is the relative activity of a micelle of aggregation number n in solution at a certain dilution.

The standard state chemical potential of a micelle of aggregation number n , μ_n^0 , is defined as the free energy change accompanied by the formation of a dry reverse micelle R_n in solution from n isolated surfactant molecules in vacuum and pure solvent according to



In this work, the standard state is defined as a system in which each solvated monomer is at infinite dilution in solvent. Similarly, for solvent molecules, the chemical potential, μ_s , is defined as

$$\mu_s = \mu_s^0 + k_B T \ln a_s. \quad (3)$$

in terms of the standard state chemical potential μ_s^0 of the solvent and the corresponding activity coefficient, a_s . The total free energy of the solution, G , can be written

$$G = N_s \mu_s + \sum_n N_n \mu_n \quad (4)$$

$$= N_s \mu_s^0 + \sum_n \mu_n^0 + k_B T (N_s \ln a_s + \sum_n N_n \ln a_n), \quad (5)$$

where the sum over n extends over all possible surfactant aggregation numbers, N_n , and N_s is the total number of solvent molecules.

For the association reaction of adding one amphiphilic surfactant molecule to an aggregate of n surfactant molecules in solution



the associated free energy difference is given by

$$\Delta G_{n+1} = \mu_{n+1} - (\mu_n + \mu_1) \quad (7)$$

$$= \Delta\mu_{n+1}^0 + k_B T \ln \frac{X_{n+1}}{X_n X_1} + k_B T \ln \frac{\gamma_{n+1}}{\gamma_n \gamma_1} \quad (8)$$

where the difference in chemical potential for adding one surfactant to a preexisting RM of aggregation number n at standard state is

$$\Delta\mu_{n+1}^0 \equiv \mu_{n+1}^0 - (\mu_n^0 + \mu_1^0) \quad (9)$$

The activity coefficient a_n is defined in terms of the mole fraction X_n and activity coefficient γ_n at size n as $a_n = \gamma_n X_n$. It notes that because of the treatment of chemical species model, if we consider the equilibrium constant related to $\Delta\mu$, the chemical potential difference does not include the combinatorial factor in the disassociation rate constant.

Finally, using the fact that the free energy at equilibrium is $\Delta G = 0$, we obtain the final relation defining the RM size distribution

$$\frac{X_{n+1}}{X_n} = \frac{\gamma_n \gamma_1}{\gamma_{n+1}} X_1 \exp \left(\frac{-\Delta\mu_{n+1}^0}{k_B T} \right) \quad (10)$$

where X_n is the mole fraction of reverse micelles of aggregation number n , and $\Delta\mu_{n+1}^0$ is the change in chemical potential associated with the reaction in Eq. (6) taken to be at infinite dilution. As our formalism employs a thermodynamic model, the microscopic effect of molecular distinguishability is introduced only through $\Delta\mu^0$ in the computed free energy change.

Physical meaning of thermodynamic quantities

To obtain the size distribution of RMs according to Eq. (10), it is necessary to determine the free energy difference $\Delta\mu_{n+1}^0$ and activity coefficient γ_n for all physically relevant values

of n . The free energy difference $\Delta\mu_{n+1}^0$ is estimated as the free energy change associated with inserting a single surfactant molecule into a reverse micelle of aggregation number n , R_n . The activity coefficient γ_n is derived from fitting experimental solvation data to the predictions of the Debye-Huckel theory.

Consider the insertion of a surfactant molecule into a RM of given aggregation number n leading to the formation of a RM of aggregation number $n + 1$. The ratio of concentrations of the two species can be related to the change in free energy upon surfactant molecule insertion as

$$\frac{X_n}{X_1} = \left(\frac{\gamma_1}{\gamma_n}\right) (\gamma_1 X_1)^{n-1} \times \exp\left(\frac{[\sum_{i=2}^n -\Delta\mu_i^0]}{k_B T}\right) \text{ for } n \geq 2. \quad (11)$$

Characterization of the complete distribution of aggregate sizes for a RM solution at equilibrium requires evaluation of the free energy differences ΔG_1^0 , for introducing a surfactant molecule from vacuum to solvent, and ΔG_{n+1}^0 , for adding one surfactant in vacuum to a preexisting RM of aggregation number n in solvent. The latter must be determined for all thermodynamically relevant values of n .

Finally, we require the following free energy evaluation for the addition of one surfactant molecule, initially in vacuum, to a preexisting RM of aggregation number n

$$R_n^{(\text{sol})} + A^{(\text{vac})} \xrightarrow{\Delta G_{n+1}^0} R_{n+1}^{(\text{sol})}. \quad (12)$$

Because $\Delta\mu_{n+1}^0 = \Delta G_{n+1}^0 - \Delta G_1^0$ for $n \geq 1$, as determined by Eq. (6), Eq. (2), and Eq. (12), Eq. (13) may be rewritten for a vacuum solute insertion

$$\frac{X_n}{X_1} = \left(\frac{\gamma_1}{\gamma_n}\right) (\gamma_1 X_1)^{n-1} \times \exp\left(\frac{[\sum_{i=2}^n -\Delta G_i^0] + (n-1)\Delta G_1^0}{k_B T}\right) \text{ for } n \geq 2, \quad (13)$$

where $\Delta G_1^0 = \Delta\mu_1^0$. Having computed the RM size distribution in terms of the concentrations, the law of mass action can be used to relate the relative concentrations of RMs to the absolute concentration of amphiphilic surfactant as

$$\sum_n n X_n = \frac{N_{AOT}}{N_{ISO}}. \quad (14)$$

Free energy evaluation

In order to determine the free energy change upon insertion of a surfactant molecule into a preexisting micelle, we employ the energy representation (ER)^{41–43} validated through

comparison with results of the thermodynamic integration (TI) method. We briefly introduce the formally exact free energy evaluation method of thermodynamic integration (TI) followed by a discussion of the approximate energy representation method (ER).

Following the notation of Frolov⁴⁷, the potential energy function of the solute-solvent system is written

$$V(\mathbf{r}_s, \mathbf{r}_w) = \Phi(\mathbf{r}_w) + v(\mathbf{r}_s, \mathbf{r}_w) \quad (15)$$

consisting of the solvent-solvent potential $\Phi(\mathbf{r}_w)$ and full coupling solute-solvent potential $v(\mathbf{r}_s, \mathbf{r}_w)$, where \mathbf{r}_s represents the configuration of the solute molecule and \mathbf{r}_w the configuration of the solvent molecules. We assume the λ -dependent solute-solvent interaction is linearly modulated by parameter λ as

$$V(\mathbf{r}_s, \mathbf{r}_w; \lambda) = \Phi(\mathbf{r}_w) + u_\lambda(\mathbf{r}_s, \mathbf{r}_w) = \Phi(\mathbf{r}_w) + \lambda v(\mathbf{r}_s, \mathbf{r}_w) \quad (16)$$

where $\lambda = 0$ represents the pure solvent system $V(\mathbf{r}_s, \mathbf{r}_w; \lambda = 0) = \Phi(\mathbf{r}_w)$ and $\lambda = 1$ represents the full interaction between solute and solvent $V(\mathbf{r}_s, \mathbf{r}_w; \lambda = 1) = \Phi(\mathbf{r}_w) + v(\mathbf{r}_s, \mathbf{r}_w)$.

Thermodynamic Integration (TI) approach

The solvation free energy of the solute can be written using Kirkwood's charging formula

$$\begin{aligned} \Delta\mu &= G_{u_{\lambda=1}}(\mathbf{r}_s, \mathbf{r}_w) - G_{u_{\lambda=0}}(\mathbf{r}_s, \mathbf{r}_w) \\ &= \int_0^1 d\lambda \int d\mathbf{r}_s d\mathbf{r}_w \frac{\partial u_\lambda(\mathbf{r}_s, \mathbf{r}_w)}{\partial \lambda} \rho_\lambda(\mathbf{r}_s, \mathbf{r}_w) = \left\langle \frac{\partial u_\lambda(\mathbf{r}_s, \mathbf{r}_w)}{\partial \lambda} \right\rangle_\lambda \end{aligned} \quad (17)$$

which forms a popular foundation for thermodynamic integration (TI). The quantity $\rho_\lambda(\mathbf{r}_s, \mathbf{r}_w)$ is the normalized classical density distribution corresponding to a potential energy of interaction given by Eq. (16) for a particular value of λ . In TI, knowledge of intermediate states between $\lambda = 0$ and $\lambda = 1$ is required for evaluation of the λ integral. As such, the ensemble average of $\partial u_\lambda / \partial \lambda$ is required for each value of λ . The state of the inserted solute is restricted to the vacuum state in Eq. (12). An effective parameterization of $V(\mathbf{r}_s, \mathbf{r}_w; \lambda)$ and sampling at the endpoints and intermediate states is essential to the success of this approach.

Energy Representation (ER) method

An alternative to the formally exact TI approach is the approximate energy representation (ER) method. In the ER method, integration over configuration space of the solute and

solvent is replaced by integration over the interaction energy between solute and solvent. The classical density distribution $\rho_\lambda(\mathbf{r}_s, \mathbf{r}_w)$ is replaced by a probability density of observing specific values of the interaction potential

$$\rho_{sw,\lambda}(\epsilon) = \sum_{i=1}^{N_w} \delta(v(\mathbf{r}_s, \mathbf{r}_w) - \epsilon) \quad (18)$$

where the energy coordinate is defined as $u_\lambda(\epsilon) = \int_{-\infty}^{\infty} d\mathbf{r}_s d\mathbf{r}_w \delta(v(\mathbf{r}_s, \mathbf{r}_w) - \epsilon) u_\lambda(\mathbf{r}_s, \mathbf{r}_w)$. The completeness and equivalence of the energy representation to the phase space representation are supported by the Kohn-Sham density functional theorem. In the ER method, information for parameterizing the energy density and potential of mean force is obtained from computer simulation.

In the ER method formalism, the formally exact result for $\Delta\mu$ in Eq. (17) may be reformed as

$$\begin{aligned} \Delta\mu &= \int_0^1 d\lambda \int d\mathbf{r}_s d\mathbf{r}_w \frac{\partial u_\lambda(\mathbf{r}_s, \mathbf{r}_w)}{\partial \lambda} \rho_\lambda(\mathbf{r}_s, \mathbf{r}_w) \\ &= \int_{-\infty}^{\infty} d\epsilon \rho_{sw,\lambda=1}(\epsilon) \epsilon - \int_0^1 d\lambda \int_{-\infty}^{\infty} d\epsilon \frac{\partial \rho_{sw,\lambda}(\epsilon)}{\partial \lambda} u_{sw,\lambda}(\epsilon), \end{aligned} \quad (19)$$

where $u_{sw,\lambda=1}(\epsilon) = v_{sw}(\epsilon) = \epsilon$ from the definition of the energy coordinate. The first term corresponds to the contribution of the solute-solvent self energy. To evaluate the second term, we introduce an auxiliary function $\omega_{sw,\lambda}$, which is the analogue of the indirect part of the potential of mean force and defined through the relation

$$\rho_{sw,\lambda}(\epsilon) = \rho_{sw,\lambda=0}(\epsilon) \exp \left[-\beta(u_{sw,\lambda}(\epsilon) + \omega_{sw,\lambda}(\epsilon)) \right], \quad (20)$$

The function $\omega_{sw,\lambda}(\epsilon)$ captures the many-body indirect interaction between solute and solvent.

Rewriting the energy density as

$$\rho_{sw,\lambda}(\epsilon) = \lambda \rho_{sw,\lambda=1}(\epsilon) + (1 - \lambda) \rho_{sw,\lambda=0}(\epsilon). \quad (21)$$

and given the potential of mean force and direct interaction energy $u_{sw,\lambda}(\epsilon)$, we can transform the second term in Eq. (19) as

$$\mathcal{F} [\rho_{sw,\lambda}(\epsilon), u_{sw,\lambda}(\epsilon)] \equiv - \int_0^1 d\lambda \int_{-\infty}^{\infty} d\epsilon \frac{\partial \rho_{sw,\lambda}(\epsilon)}{\partial \lambda} u_{sw,\lambda}(\epsilon) \quad (22)$$

$$\begin{aligned} &= k_B T \int d\epsilon \left[(\rho_{sw,\lambda}(\epsilon) - \rho_{sw,\lambda=0}(\epsilon)) - \rho_{sw,\lambda}(\epsilon) \ln \frac{\rho_{sw,\lambda}(\epsilon)}{\rho_{sw,\lambda=0}(\epsilon)} \right. \\ &\quad \left. - \beta(\rho_{sw,\lambda}(\epsilon) - \rho_{sw,\lambda=0}(\epsilon)) \int_0^1 d\lambda \omega_{sw,\lambda}(\epsilon) \right], \end{aligned} \quad (23)$$

where we have used the identity

$$\frac{\partial \rho_{sw,\lambda}(\epsilon)}{\partial \lambda} = \rho_{sw,\lambda}(\epsilon) - \rho_{sw,\lambda=0}(\epsilon). \quad (24)$$

Finally, the excess chemical potential in the energy representation can be written

$$\mu_{ex} [\rho_{sw,\lambda}(\epsilon), u_{sw,\lambda}(\epsilon)] = \int_{-\infty}^{\infty} d\epsilon \rho_{sw,\lambda}(\epsilon) \epsilon - \mathcal{F} [\rho_{sw,\lambda}(\epsilon), u_{sw,\lambda}(\epsilon)] \quad (25)$$

This equation is exact if the potential mean force $\omega_{sw,\lambda}(\epsilon)$ is exact. However, in practice as in all integral equation theories $\omega_{sw,\lambda}$ must be treated approximately. As such, the accuracy of this method depends on how well the approximate form of the potential of mean force captures many body interactions that are not included in the direct interaction of solute and solvent.

The pioneering work of Matubayasi and Nakahara provides guidance on the best choice of functional forms for the potential of mean force $\omega(\epsilon)$. It is recommended that a combination of (1) a hypernetted chain (HNC) equation inspired contribution for $\omega^{(HNC)}(\epsilon) < 0$, capturing attractions, is combined with (2) a Percus-Yevick (PY) equation inspired term for $\omega^{(PY)}(\epsilon) > 0$, capturing repulsions. The sign of $\omega(\epsilon)$ shows the clear boundary between the repulsions and attractions. By exploiting this insight, the λ integral can be heuristically weighted through a function $\alpha(\epsilon)$ as

$$\beta \int_0^1 d\lambda \omega_{sw,\lambda}(\epsilon) \approx \alpha(\epsilon) \cdot F_{\omega_1}(\epsilon) + (1 - \alpha(\epsilon)) \cdot F_{\omega_0}(\epsilon), \quad (26)$$

where $F_{\omega_1}(\epsilon) = \beta \int_0^1 d\lambda \omega_{sw,\lambda=1}(\epsilon)$ and $F_{\omega_0}(\epsilon) = \beta \int_0^1 d\lambda \omega_{sw,\lambda=0}(\epsilon)$. The specific form of $\alpha(\epsilon)$ is discussed in detail elsewhere^{42,47}. In this way, the λ integral required for the determination of the excess chemical potential in the ER method may be evaluated solely based on knowledge of the energy density at the endpoints $\lambda = 1$ and $\lambda = 0$ through $\rho_{sw,\lambda=1}(\epsilon)$ and $\rho_{sw,\lambda=0}(\epsilon)$. In this way, the simulation of intermediate states for the system is avoided, providing a distinct advantage over the TI method. However, many-body effects are approximately included. In systems for which many body interactions are important, the accuracy of this method is expected to diminish.

System setup

The goal of this study is to describe the equilibrium size distribution for dry RMs formed by AOT surfactant in isooctane solvent. This requires the calculation of the chemical po-

tential difference $\Delta\mu_{n+1}^0$ for all thermodynamically relevant values of n . To compute these quantities using the ER method, we must simulate dry micellar systems for a wide variety of aggregate numbers.

We first prepared each initial configuration of a RM system of a given composition. Initial conditions were defined by spherically arranged configurations of surfactant molecules created using the Packmol program⁴⁸. The isooctane solvent molecules were arranged surrounding the RM. The energy of each system was minimized using the steepest descent algorithm to remove bad contacts. Each system was subsequently equilibrated in the NVT ensemble with velocity rescaling for 300 ps, followed by equilibration in the NPT ensemble with Nose-Hoover and Parrinello-Rahman coupling for 300 ps. Finally, each system was equilibrated at 300 K and 1 bar to find an average density of approximately $0.7g/cm^3$. Production runs were subsequently performed for 70 ns.

Equilibration of the system was followed by production runs in the NVT ensemble using the GROMACS program (version 5.1)^{49–51}. In those simulations, the time step was 2 fs using bond length constraints through LINCS for all hydrogens bonded to heavy atoms. Electrostatic calculations were performed using the Particle Mesh Ewald method with 1.2 Å cutoff in a rectangular box. The van der Waals term was calculated using a potential switch between 1.0 and 1.2 nm. We employed the modified CHARMM force field developed by Abel and coworkers⁵² for AOT surfactant and isooctane solvent molecules. A complete list of systems studied is provided in Table I. Images were rendered by VMD⁵³. For analysis involving the ER method the ERMOD program (version 0.3.4) was employed⁵⁴. Statistical averaging was performed using the R program package^{55,56} and library⁵⁷.

For applications of the energy representation method, the last 50ns of each production run of the solution system was used for with a sampling interval of 10 ps for Eq. (9). The reference system excluded one AOT molecule from the solution system and sampling was performed over the last 50 ns of dynamics using an interval of 4 ps. The intermolecular structure of the inserted AOT molecule was prepared using a simulation of an isolated AOT molecule in isooctane solvent performed for the last 5 ns with a sampling interval of 0.4 ps. To construct distributions in the reference state, test-particle insertion of the solute was performed 10,000 times for each reference configuration. The center-of-mass of the test particle was selected to be in the region from the center-of-mass of the AOT aggregate to the radius of gyration R_g of the AOT aggregate, $0 < r < R_g$.

In the analysis of trajectories, the simulated RM shape was taken to be ellipsoidal. For a RM of total mass, M , the principal moments of inertia, $I_1 > I_2 > I_3$, are related to the semiaxes a, b, c defined as

$$I_1 = \frac{1}{5}M(a^2 + b^2), a^2 = \frac{5}{2M}(I_1 + I_2 - I_3) \quad (27)$$

$$I_2 = \frac{1}{5}M(a^2 + c^2), b^2 = \frac{5}{2M}(I_1 - I_2 + I_3) \quad (28)$$

$$I_3 = \frac{1}{5}M(b^2 + c^2), c^2 = \frac{5}{2M}(-I_1 + I_2 + I_3) \quad (29)$$

For the semiaxes $a > b > c$ of an ellipsoid, the asphericity A_s is defined

$$A_s = \frac{\lambda_z^2 - \frac{1}{2}(\lambda_x^2 + \lambda_y^2)}{\lambda_z^2}, \quad \lambda_x^2 \leq \lambda_y^2 \leq \lambda_z^2, \quad (30)$$

where $A_s = 0$ for a sphere. The radius of gyration R_g is defined as

$$R_g^2 = \frac{\sum_i m_i (r_i - r_{com})^2}{M} = \frac{a^2 + b^2 + c^2}{5}, \quad (31)$$

where m_i is the mass of atom i at distance r_i from the RM's center-of-mass r_{com} . This result assumes a uniform density. The average radius of the RM is $(abc)^{\frac{1}{3}}$ corresponding to the radius of a sphere with the same volume.

RESULTS

Structures of the simulated dry micelle aggregates were characterized in terms of the radius of gyration and asphericity, which are related to the overall aggregate size and shape, and mass distribution functions, which provide insight into the internal structure of the micelle. Table I lists the compositions of each simulated system, defined by the number of AOT molecules and the overall number of isooctane molecules used in the free energy evaluation. As expected, the radius of gyration increases as the aggregate number increases, while the asphericity approaches zero with increasing aggregate size.

A principal result of this study is the determination of the differential chemical potential, $\Delta\mu_{n+1}^0$, representing the free energy change at standard state for the process of adding one surfactant to an existing micelle aggregate, $R_{n-1} + A \Rightarrow R_n$. The results derived from Eqs. (10) and (19) are shown in Fig. 1 as a function of aggregate number n . Key quantities related to the change in free energy were computed approximately using the ER method and interpolated for intermediate values of the aggregation number, n .

Error bars were computed using the following scheme. (1) Averages were calculated for the solution system with statistical error measured by splitting the trajectory into ten block subtrajectories. (2) Energy distributions were constructed in which the energy was discretized, respecting a mesh size of $\Delta\epsilon$. The mesh size was increased from a chosen size to that value multiplied by a factor of 1, 2, 3, ..., and 10, e.g. $\Delta\epsilon = 0.001, 0.002, \dots$, and 0.01 kcal/mol . The solvation free energy difference computed for each mesh size was used as a measure of the mesh size error. Differences in free energy between trajectory blocks using the same mesh size were found to be at most 2.0 kcal/mol for all aggregate sizes. As an example, the composite error of roughly 12 kcal/mol for $n=90$ is composed of the statistical error in trajectory average of 2.0 kcal/mol and the error associated with mesh size dependence of $10. \text{ kcal/mol}$.

The overall profile of $\Delta\mu_{n+1}^0$ shows a rapid decrease with increasing aggregate size for small n , followed by a minimum near $n = 20$ and subsequent increase to intermediate values near $n = 30$. As n increases further, a broad second minimum is identified followed by a plateau for larger n . Insight into the non-monotonic behavior of the free energy is provided by the representative structures associated with the two minima and intermediate maximum. Clearly, the dry micelle aggregates possess a structure that is not well captured by the radius of gyration and asphericity alone.

Further insight into the structure of aggregates of varying size is provided by analysis of the internal mass density distribution. Fig. 2 depicts the mass density of each micelle component as a function of distance from the center-of-mass of the aggregate. This figure suggests that the abrupt change in free energy between $n = 20$ and $n = 30$ results from the aggregation of head groups near the center-of-mass of the dry micelle.

For $n = 20$ it is possible to colocalize head group atoms near the center-of-mass leading to a peak in the sulfur atom mass distribution near 8 \AA , and oxygen and sodium peaks near 8 \AA . As the representative inset structure shows, however, the head groups form a folded “taco shell” conformation as opposed to a spherical aggregate. The head group shows a sharp peak in its distribution at 1 nm . This allows for the formation of a compact micelle structure with head groups gathered near the micelle center while minimizing head group repulsion. A few isooctane molecules were found to be enclosed in the core formed of AOT head groups rather than AOT tails. Such penetration is possible as a result of the small difference in surface tension between organic solvent, $25 - 35 \text{ mN/m}^{10,30}$, and AOT, 30 mN/m^{58} . (This

can be compared to the value for water, 70 mN/m.) Given the small difference in surface tension, structural fluctuations that allow the aggregate center to have both AOT tail and isooctane solvent are possible.

For $n = 30$, head group repulsion leads to a more complex dry micelle structure. While the overall asphericity of the aggregate is not great, the internal structure associated with the arrangement of surfactant head groups creates two joined toroidal forms. This internal structure reflects a mass distribution with a strong peak in the density of AOT tail group atoms near 5 \AA , with a wider sulfur atom distribution at a distance of 6 \AA to 12 \AA . This suggests that the observed shift in the peak position of the AOT sulfur atom makes an important contribution to the free energy surface maximum. In contrast, the identity of a core molecule, as a surfactant tail or a solvent molecule, has little effect when compared to the electrostatic energy resulting from head group interactions. This complex internal structure of the micelle is reflected in a peak in the differential chemical potential, $\Delta\mu_{n+1}^0$.

As the micelle size increases further to $n = 60$, a second morphological transition occurs leading to a micelle composed of a spherical shell of head groups, reflected by a peak in the sulfur atom density between 14 \AA and 17 \AA . There is a substantial density of surfactant tail groups and isooctane molecules in the center of the micelle, suggesting that the micelle core is composed of non-polar molecules in contrast to the structure of a “wet” reverse micelle. This arrangement of surfactant head groups, distributed over a spherical shell containing surfactant tails groups as well as non-polar solvent, is reflected in a decrease in $\Delta\mu_{n+1}^0$. After $n = 60$, the differential chemical potential is observed to plateau at a constant value within the error bars of our computed values.

The observed penetration of non-polar solvent molecules has been proposed for wet reverse micelles in benzene solvent based on NMR experiments⁵⁹. However, the inclusion of non-polar solvent in the core of dry AOT RMs has not been previously observed or proposed. Moreover, the high mobility of solvent molecules after the formation of the micelle is consistent with the unfavorable entropy and enthalpy differences observed in experiment. In normal micelles, after micelle formation, fluctuation in surfactant molecules decreases while fluctuations in water molecules increases, leading to an increase in entropy during micellization. However, in dry RM formation, micellization causes surfactant molecules to lose translational entropy, leading to a decrease in total entropy. This provides an explanation for the negative entropy change associated with RM micellization. It appears that

the structure of larger dry RMs balances the advantage of aggregation of surfactant while minimizing the penalty of electrostatic repulsion among charged anionic head groups. The result is that upon reaching a critical size, the RM is able to form of spherical structure characterized by a shell of head groups, dressed in the non-polar surfactant tails, encapsulating a non-polar solvent core and surrounded by bulk non-polar solvent. This addresses the long-standing question regarding how anionic AOT surfactant molecules can form reverse micelle structures in non-polar solvent in the absence of a cosurfactant or water.

Considering the activity coefficients, for the AOT reverse micelle system we expect that molecular charging will require higher energy cost in non-polar as opposed to water solvent. In particular, the anionic AOT molecule strongly mediates such charging in non-polar solvent^{60,61}, and we expect that electrostatic interaction among RMs strongly affects their behavior. Similar electrostatic interaction was examined in various experiments with explained by Debye-Huckel theory and its screened potential form⁶²⁻⁶⁵. As such, we assume the validity of the Debye-Huckel theory which suggests that

$$\log \left(\frac{\gamma_n \gamma_1}{\gamma_{n+1}} \right) \propto \alpha n. \quad (32)$$

We assume the simplest relation between aggregate size and electrostatic interaction that the charge and size are proportional to each other. Even if only a few charged RMs are present in solution, electrostatic interaction between ions will be essential in characterizing the properties of the solution. Under this scaling assumption, the number of parameters is limited to α only, which will be dependent on conditions such as the dielectric properties of the medium, ionic strength reflecting by head group and counter ion charge, and temperature. This is a rather crude approximation as we employ a single mean activity coefficient for each aggregate size. Our motivation was to limit the number of adjustable parameters involved in the model. This scaling is expected to be valid in dilute neutral electrolyte solution with the concentration on the order of 0.1 M. To investigate the effect of varying activity coefficient, we investigated the variation in the activity coefficient for systems ranging from the pure monomer state, corresponding to the experimental phase at lower AOT concentrations, to the liquid crystal state, associated with higher AOT concentrations. This allows us to probe the effect of interaggregate interactions for a given size distribution.

Fig. 3(a) depicts the size distribution for $\alpha \simeq 0$ which is dominated by monomers. Fig. 3(d) shows the corresponding activity coefficient ratio which is near zero. Fig. 3(b)

shows a sharp peak in the micelle size distribution near $n = 28$ corresponding to the critical micelle concentration (CMC) value. Here α is set to -2 for the ratio of activity coefficients as shown in Fig. 3(e). The size distribution for the ideal solution is shown in Fig. 3(c) with corresponding ratio of activity coefficients set to unity as shown in Fig. 3(f). In this system, all surfactant molecules $n = 100$ in the system aggregate to form the largest possible aggregate representing an insoluble state of a liquid crystal. This result is in agreement with conclusions drawn in a previous theoretical work¹⁹. As the results in Fig. 3 demonstrate, variations in the activity coefficient leads to distinct changes in the character of the solution composition, ranging from monomers to insoluble aggregates and including a sharply peaked distribution near the CMC. The actual solution of AOT surfactant in isooctane solvent must balance electrostatic repulsions and entropic contributions in the equilibrium state⁶⁰. This implies that larger aggregates have strong electrostatic repulsion and monomer and smaller aggregates are stabilized by entropy. These results suggest that the interaction between AOT aggregates is sensitive to AOT surfactant concentration.

We now consider the balance in terms that determines the mole fraction of aggregates of size n . We rewrite the size distribution relation reflected in Eq. (10) in terms of monomer distribution. By substituting the activity term and multiplying the smaller size relations iteratively, Eq. (10) is transformed into

$$\log X_n = n \log X_1 + \alpha \sum_{i=1}^{n-1} i - \frac{\sum_{i=2}^n \Delta\mu_i^0}{k_B T}. \quad (33)$$

This equation displays how the free energy surface and activity coefficient parameter determine the mole fraction of aggregates of size n . To better appreciate the aggregate size distribution depicted in Fig. 3(b), the balance of each term in Eq. (33) is shown in Fig. 4. α was set to -2 and the total mole fraction was conserved at the CMC for the X_1 term. These separate contributions show that the finite aggregation at $n=28$ occurs due to the convex nature of the cumulative sum of free energy from the local minimum at $n = 20$ through the local maximum at $n = 30$. The narrow distribution is a direct reflection of the height of the barrier separating the local minima. The height of the barrier is on the order of several tens of $kcal/mol$ resulting in a relatively monodisperse aggregate size distributions.

Figure 5 shows the micelle size distribution for surfactant concentration varying from 0.1 CMC to 5 CMC. The slope α in the activity relation has been interpolated between the value of the dispersed state and the micelle state in Fig. 3 (b). To capture this behavior,

the functional form must show a sudden increase near the threshold value. As such, we have employed an interpolation between the dispersed state and micelle state using a sigmoidal function to reproduce the phenomenon of a sudden occurrence of micelles near the CMC as

$$\alpha(x) = A + \frac{(B - A)}{[1 + \exp(-C(x - D))]^{(E-1)}} \quad (34)$$

where we have set $A = -30$, $B = -2$, $C = 10^6$, $D = CMC$, and $E = 35$. These resulting micelle size distributions are narrow with width $\Delta n = 2$, which is consistent with the experimental results for an AOT/alkane system²⁸. Importantly, the prediction of a small change in the mean aggregate size after the CMC is reached is also observed in experiment²⁹. This implies that near the CMC the activity coefficient abruptly increases from near zero as a function of concentration, and subsequently may be considered to be essentially constant. This suggests that while normal micelle formation is dominated by the free energy difference between dispersed aggregated states and micelle states, in the formation of dry micelles the interactions among aggregates will be a driving force that determines the equilibrium state. The importance of micelle-micelle interactions for the observed phase transition near the CMC has been previously suggested⁶⁶⁻⁶⁹. However, to our knowledge, no previous theory has captured the difference in free energy associated with intermicelle interaction.

For solutions of normal micelles, it is observed that as the concentration increases near the CMC the size distribution shows a gradual increase from monomer to normal micelle.⁷⁰ For the dry reverse micelle, we observe that surfactant AOT molecules make a sudden transition from monomer to micelle aggregate near the CMC. Such an abrupt transition from the monomer regime to the micelle state has been anticipated but never observed in normal micelle solutions. As such, this represents a striking difference between the thermodynamics of normal micelle formation and the formation of dry RMs. This observed difference results from the magnitude of variation in $\Delta\hat{\mu}_n^0$ over several $kcal/mol$ in normal micelles and several tenths of a $kcal/mol$ in the case of dry RMs. Variations in enthalpy over tenths of a $kcal/mol$ have been observed in an experimental study of AOT micellization in alkane solvent¹⁶. As the enthalpy change in surfactant AOT micellization depends on the choice of solvent, we expect a corresponding dependence of the RM size distribution on the choice of solvent.

Note that the observed transition is invariant to the specific nature of the function used to model the slope parameter α . Fig. 6 shows the continuous change in the micelle size distribution as a function of *slope*. The mean size of the dry micelle is observed to depend

on the slope value, while the point at which AOT molecules form aggregates from monomers is relatively insensitive to slope values. This suggests that the sigmoidal function employed in this work to interpolate values of the activity coefficient up to the CMC, given by Eq. (34), does not influence the specific regime in which the first dry RM is observed.

In addition, the mean aggregate size, N_{agg} , for the distributions gradually increases from a dispersed state $N_{agg} = 1$ through $N_{agg} = 30$, with varying slope ranging from $slope = -22$ to -2 . This behavior is in agreement with the experimentally reported values of surfactant AOT ranging from $N_{agg} = 30$ in *n*-octane, to 37 in *n*-decane, to 44 in *n*-dodecane^{27,71}. This implies that if the activity coefficient gradually increases as a function of AOT concentration, the system displays no CMC in this region. Consider the gradual increase observed in the mean aggregate size, which shows a sharp transition for 30 to 65. Moreover, regions of higher AOT concentration may stand beyond the dilute solution limit. These specific aggregate sizes correspond to local maximum values in μ_{n+1}^0 . We must note, however, that our results for the mean free energy are accompanied by large error bars. As such, the transition from 30 to 80 may be an artifact. Assuming that the free energy surface is constant after $n = 50$ in μ_{n+1}^0 , our results imply that the surfactant AOT molecules become insoluble near ($N_{agg} = 100$), in agreement with the liquid crystal state of the ternary phase diagram along the AOT/isooctane line⁷².

DISCUSSIONS

In this study, we have obtained the size distribution of dry surfactant AOT aggregates in non-polar solvent. The free energy of the isolated aggregate formation was evaluated through free energy simulation using the energy representation method. The obtained free energy surface demonstrates that small surfactant aggregates can form, resulting in a dense surfactant head group region. In surfactant aggregates, the AOT heads groups disperse from the center-of-mass of the aggregate and create a core region that can accommodate isooctane solvent molecules. The spontaneous formation of a “pore-like” structure allows for minimization of head group repulsion and the formation of stable dry RM aggregates. In modeling the interaction of dry RM aggregates, we employed the Debye-Huckel theory scaling relation for variation in the activity coefficient with increasing aggregate number in dilute solution. It was observed that depending on the degree of interaction, the dry

RM size distribution displayed a variety of aggregate forms including soluble dry micelles and insoluble aggregates. A prediction of the theory is that dry RM formation requires very small activity coefficients $\gamma_n \approx 0$ for larger aggregates and n , but $\gamma_n \neq 0$ for smaller aggregates and $n < 10$.

In previous theoretical work, the existence of a CMC for dry RM formation was denied. We believe this was a direct result of the inability to accurately describe the free energy of solution of dry RM aggregates assuming ideal solution conditions. Recently, Kislenko and Razumov⁷³ investigated dry RM formation in an AOT/hexane system using thermodynamic integration and all-atom simulations. Their free energy surface showed features similar to the dependence reported here. However, the final finite RM concentration was found to be roughly twenty orders of magnitude smaller than that of the monomer, and much lower than that of the largest aggregates due to an ideal solution condition. This demonstrates that one must account for interactions between surfactant aggregates. In this work, we obtained the formation free energy of aggregates through free energy evaluation using the energy representation method. The mean aggregate size was found to increase as a function of total surfactant concentration in a way that depends on variation in the activity coefficient.

If the activity coefficient displays a weak increase as a function of concentration, the mean aggregate size displays a gradual increase from $n = 1$ to 30. This dependence is determined by the variation in differential chemical potential, $\Delta\mu$, as a function of dry RM size. For aggregates larger than 30, the mean aggregate size was observed to undergo an abrupt transition to much larger aggregate sizes. This dependence results from the variation in the monomer activity coefficient with an increase from 0 (an extreme “salt-out” condition) to 1 (an ideal solution condition).

From this variation, we conclude that the interaction of surfactant aggregates in oil solvent plays a major role in dry RM formation. This stresses the importance of capturing the dynamic equilibrium underlying the established equilibrium aggregate size distribution. This behavior is quite distinct from normal micelle formation, approximately expressed using ideal solution conditions. Moreover, our results suggest why calorimetry experiments²⁰ have failed to observe the existence of a CMC for dry AOT surfactant RM formation.

The free energy surface suggests that there will be only a minor change in aggregate size distribution as a result of a modest increase in temperature of the RM phase. This is observed in experiment. Note that at the threshold temperature separating the RM

and liquid crystal states intermicelle interaction is found to be critical. We observe that a change in temperature cannot trigger a shift in the equilibrium state between a distribution dominated by surfactant monomers and one defined by aggregates. As such, we do not observe a maximum in the heat capacity as a function of surfactant concentration.

Our results also suggest a reason for the observed deviation in mean aggregate size in experiment. In larger aggregates $n > 20$, we observed the penetration of isooctane molecules in the center of the surfactant aggregate, with the solvent “core” surrounded by aliphatic tail groups of the AOT surfactant. In experimental estimates of the mean size of surfactant aggregates, it is typically assumed that the aggregate is solely composed of AOT surfactant molecules. This assumption may lead to an overestimate in the aggregation number. In the case of dry RM formation by AOT surfactant in isooctane solvent, we estimate that this overestimate of the aggregation number can be as large as 10. In addition, many experimental studies assume a spherical surfactant aggregate. However, we observe that due to the formation of the solvent core large aggregates may deviate from a spherical shape. Moreover, an inclusion of oil is an origin of the observed decrease in entropy upon micellization in non-polar solvent.

The change in chemical potential μ_n^0 is computed using the energy representation method in the infinite dilution limit. As such, the theory may appear to be that of an “ideal solution” in which intermicelle interactions are ignored. However, as we employ activity coefficients γ_i that differ from unity, the solution is “non-ideal”. The ideal solution is defined in terms of the enthalpy contribution in the absence of solute-solute interaction and entropy contribution equivalent to the ideal entropy at any standard state. As such, we argue that intermicellar interactions are included implicitly through the activity coefficients.

Consider the reaction $A_n + A \Rightarrow A_{n+1}$. The equation $\mu_n = \mu_n^0 + kT \ln a_n = \mu_n^0 + kT \ln(\gamma_n X_n)$ demonstrates that the free energy consists of two terms, an ideal contribution, $\mu_n^{ideal} = \mu_n^0 + kT \ln X_n$, and non-ideal contribution, $\mu^{non-ideal} = kT \ln a_n$. The non-ideal contribution can be written $kT \ln \gamma_n = (H_n - H_n^{ideal}) - T(S_n - S_n^{ideal})$, where H_n and S_n are the enthalpy and entropy of a micelle of size n , respectively. If the size and morphology of a micelle of size $n + 1$ do not show significant change between the standard state and actual solution state, we expect the entropic contribution to the non-ideal component of $\ln(\gamma_n)$ will be modest. In contrast, in the standard state enthalpic contributions from intermicelle interactions involving aggregates of size n and $n + 1$ are not expected to be significant com-

pared to the contribution from micelle-solvent interaction. However, at higher concentration the binding reaction is completed in the presence of other micelles. As such, the major contribution of $H_n - H_n^{ideal}$ to γ_n is due to the interaction among micelles. (The interaction between micelles of size n and solvent is already included in H_n^{ideal} .) No other difference exists between the chemical potential of the standard state, μ_n^0 , and the actual state, μ_n . This reasoning demonstrates that the change in activity coefficient includes contributions from intermicelle interaction as a function of AOT concentration.

We make one further observation. We have employed the chemical species model for the derivation of our thermodynamic relations. An assumption of the model is that the activity coefficient γ_n is a function of the distribution of sizes of other micelles present in the solution or that

$$\ln \gamma_n = f([RM_1], [RM_2], \dots, [RM_{n-1}], [RM_{n+1}], \dots, [RM_N]) \quad (35)$$

rather than $\ln \gamma_n = f([AOT])$ as found in solute-solute interaction. On the other hand, as the total concentration of surfactant, $[AOT]$, increases, it will change the distribution of micelle sizes and the values of $[RM_1], [RM_2], \dots, [RM_{n-1}], [RM_{n+1}], \dots, [RM_N]$, leading to a change in the activity for each micelle size. This suggests that γ_n should vary explicitly as a function of surfactant concentration for wider regions of total $[AOT]$. Such strong intermicelle interaction is observed in experiments^{74,75} related to mass transport and percolation in wet RMs.

The validity of our activity model is supported by the fact that it can capture essential features of the experimental results, including the narrow aggregate size distribution and predicted stable mean aggregate size. While our model can capture the feature of a mean aggregate size between 30 and 60, we appreciate that improvements could be made to enhance the predictive ability of the model and provide more direct interpretation of the results. We consider our work to be a reasonable and useful first approximation to a more complete analysis.

In summary, our results suggest that in non-polar solvent, molecular interactions between surfactant aggregates and non-polar solvent molecules play an important role in establishing equilibrium for dry RM formation due to the fact that surfactant molecules demonstrate a weak ability to associate in non-polar solvent. Addition of water molecules to a dry RM system leads to the formation of a wider variety of stable RMs. The extension of the formalism developed in this work to the case of “wet” RMs, such as those found in a ternary

AOT/isooctane/water system, should allow for a similar characterization of the equilibrium RM size distribution, a goal that has existed for many years as an important challenge to the field.

ACKNOWLEDGMENTS

We gratefully acknowledge the National Science Foundation (CHE-1362524) for the generous support of our research. JES thanks the Japan Society for the Promotion of Science (JSPS) for the support provided by an Invitation Fellowship (L13523) and BRIDGE Fellowship (BR160401) hosted at Nagoya University.

REFERENCES

- ¹D.-H. ZHANG, Z. GUO, X.-Y. DONG, and Y. SUN, *Biotechnol Progress* **23**, 108 (2007).
- ²T. HINO, Y. KAWASHIMA, and S. SHIMABAYASHI, *Adv. Drug Deliv. Rev.* **45**, 27 (2000).
- ³H. OKOCHI and M. NAKANO, *Adv. Drug Deliv. Rev.* **45**, 5 (2000).
- ⁴S. HIGASHI and T. SETOGUCHI, *Adv. Drug Deliv. Rev.* **45**, 57 (2000).
- ⁵Y. NISHII, T. KINUGASA, S. NII, and K. TAKAHASHI, *J. Memb. Sci.* **195**, 11 (2002).
- ⁶N. V. NUCCI, K. G. VALENTINE, and A. J. WAND, *J. Magn. Reson.* **241**, 137 (2014).
- ⁷I. DODEVSKI, N. V. NUCCI, K. G. VALENTINE, G. K. SIDHU, E. S. OBRIEN, A. PARDI, and A. J. WAND, *J. Am. Chem. Soc.* **136**, 3465 (2014).
- ⁸N. GALAMBA, *J. Phys. Chem. B* **117**, 2153 (2013).
- ⁹N. GALAMBA, *J. Phys. Chem. B* **118**, 4169 (2014).
- ¹⁰M. J. SCHICK, *Nonionic surfactants: physical chemistry*, CRC Press, 1987.
- ¹¹R. H. ARANOW and L. WITTEN, *J. Phys. Chem.* **64**, 1643 (1960).
- ¹²R. H. ARANOW and L. WITTEN, *J. Chem. Phys.* **43**, 1436 (1965).
- ¹³K. SHIRAGA, T. SUZUKI, N. KONDO, and Y. OGAWA, *J. Chem. Phys.* **141**, 235103 (2014).
- ¹⁴H. S. FRANK and M. W. EVANS, *J. Chem. Phys.* **13**, 507 (1945).
- ¹⁵H.-F. EICKE and H. CHRISTEN, *Helv. Chim. Acta* **61**, 2258 (1978).
- ¹⁶K. MUKHERJEE, S. MOULIK, and D. MUKHERJEE, *Langmuir* **9**, 1727 (1993).
- ¹⁷E. RUCKENSTEIN and R. NAGARAJAN, *J. Phys. Chem.* **84**, 1349 (1980).

- ¹⁸P. EKWALL, L. MANDELL, and K. FONTELL, *J. Colloid Interface Sci.* **33**, 215 (1970).
- ¹⁹A. WOOTTON, F. PICAVER, P. HARROWELL, M. TOKUYAMA, I. OPPENHEIM, and H. NISHIYAMA, The Structure and Thermodynamic Stability of Reverse Micelles in Dry AOT / Alkane Mixtures, in *AIP Conf. Proc.*, volume 982, pp. 289–294, AIP, 2008.
- ²⁰R. TANAKA, *Journal of Japan Oil Chemists’ Society* **41**, 82 (1992).
- ²¹R. TANAKA, T. YOKOYAMA, K. SAMESHIMA, and T. KAWASE, *Bull. Chem. Soc. Jpn.* **78**, 599 (2005).
- ²²K. SAMESHIMA, R. TANAKA, K. IGARASHI, and H. OOSHIMA, *J. Chem. Thermodyn.* **38**, 662 (2006).
- ²³S. H. CHEN, *Ann. Rev. Phys. Chem.* **37**, 351 (1986).
- ²⁴S. MUTO and K. MEGURO, *Bull. Chem. Soc. Jpn.* **46**, 1316 (1973).
- ²⁵K. KON-NO and A. KITAHARA, *J. Colloid Interface Sci.* **35**, 636 (1971).
- ²⁶A. KITAHARA, T. KOBAYASHI, and T. TACHIBANA, *The J. Phys. Chem.* **66**, 363 (1962).
- ²⁷S. G. FRANK and G. ZOGRAFI, *J. Pharm. Sci.* **58**, 993 (1969).
- ²⁸G. N. SMITH, P. BROWN, S. E. ROGERS, and J. EASTOE, *Langmuir* **29**, 3252 (2013).
- ²⁹G. N. SMITH, P. BROWN, C. JAMES, S. E. ROGERS, and J. EASTOE, *Colloids Surf. A Physicochem Eng. Asp.* **494**, 194 (2016).
- ³⁰M. J. HOLLAMBY, R. TABOR, K. J. MUTCH, K. TRICKETT, J. EASTOE, R. K. HEENAN, and I. GRILLO, *Langmuir* **24**, 12235 (2008).
- ³¹P. CHRISTOPHER and D. W. OXTOBY, *J. Phys. Chem.* **118**, 5665 (2003).
- ³²G. MOHAN and D. I. KOPELEVICH, *J. Phys. Chem.* **128**, 044905 (2008).
- ³³J. T. KINDT, *J. Chem. Theory Comput.* **9**, 147 (2013).
- ³⁴A. BEN-SHAUL and W. M. GELBART, *The J. Phys. Chem.* **86**, 316 (1982).
- ³⁵M. KINOSHITA and Y. SUGAI, *Chem. Phys. letters* **313**, 685 (1999).
- ³⁶M. KINOSHITA and Y. SUGAI, *J. Comput. Chem.* **23**, 1445 (2002).
- ³⁷N. YOSHII and S. OKAZAKI, *Chem. Phys, Lett.* **425**, 58 (2006).
- ³⁸N. YOSHII and S. OKAZAKI, *Chem. Phys, Lett.* **426**, 66 (2006).
- ³⁹N. YOSHII, K. IWAHASHI, and S. OKAZAKI, *J. Chem. Phys.* **124**, 184901 (2006).
- ⁴⁰N. YOSHII and S. OKAZAKI, *Cond. Mat. Phys* **10**, 573 (2007).
- ⁴¹N. MATUBAYASI and M. NAKAHARA, *J. Chem. Phys.* **113**, 6070 (2000).
- ⁴²N. MATUBAYASI and M. NAKAHARA, *J. Chem. Phys.* **117**, 3605 (2002).
- ⁴³N. MATUBAYASI and M. NAKAHARA, *J. Chem. Phys.* **119**, 9686 (2003).

- ⁴⁴C. TANFORD, *The Hydrophobic Effect: Formation of Micelles and Biological Membranes 2d Ed*, J. Wiley., 1980.
- ⁴⁵S. PUVVADA and D. BLANKSCHTEIN, *J. Phys. Chem.* **92**, 3710 (1990).
- ⁴⁶N. ZOELLER, L. LUE, and D. BLANKSCHTEIN, *Langmuir* **13**, 5258 (1997).
- ⁴⁷A. I. FROLOV, *J. Chem. Theory Comput.* **11**, 2245 (2015).
- ⁴⁸L. MARTÍNEZ, R. ANDRADE, E. G. BIRGIN, and J. M. MARTÍNEZ, *J. Comput. Chem.* **30**, 2157 (2009).
- ⁴⁹H. BERENDSEN, D. VAN DER SPOEL, and R. VAN DRUNEN, *Comput. Phys. Commun.* **91**, 43 (1995).
- ⁵⁰S. PÁLL, M. J. ABRAHAM, C. KUTZNER, B. HESS, and E. LINDAHL, Tackling Exascale Software Challenges in Molecular Dynamics Simulations with GROMACS, in *International Conference on Exascale Applications and Software*, edited by S. MARKIDIS and E. LAURE, pp. 3–27, Springer International Publishing, 2015.
- ⁵¹M. J. ABRAHAM, T. MURTOLA, R. SCHULZ, S. PÁLL, J. C. SMITH, B. HESS, and E. LINDAHL, *SoftwareX* **1**, 19 (2015).
- ⁵²S. ABEL, F. STERPONE, S. BANDYOPADHYAY, and M. MARCHI, *J. Phys. Chem. B* **108**, 19458 (2004).
- ⁵³W. HUMPHREY, A. DALKE, and K. SCHULTEN, *J. Mol. Graph.* **14**, 33 (1996).
- ⁵⁴S. SAKURABA and N. MATUBAYASI, *J. Comput. Chem.* **35**, 1592 (2014).
- ⁵⁵R CORE TEAM, *R: A Language and Environment for Statistical Computing*, R Foundation for Statistical Computing, Vienna, Austria, 2015.
- ⁵⁶R. IHAKA and R. GENTLEMAN, *J. Comput. Graph. Stat.* **5**, 299 (1996).
- ⁵⁷D. ADLER, D. MURDOCH, and OTHERS, *rgl: 3D Visualization Using OpenGL*, 2016, R package version 0.95.1441.
- ⁵⁸S. NAVE, J. EASTOE, and J. PENFOLD, *Langmuir* **16**, 8733 (2000).
- ⁵⁹C. A. MARTIN and L. J. MAGID, *J. Phys. Chem.* **85**, 3938 (1981).
- ⁶⁰M. F. HSU, E. R. DUFRESNE, and D. A. WEITZ, *Langmuir* **21**, 4881 (2005).
- ⁶¹W. H. BRISCOE and R. G. HORN, *Langmuir* **18**, 3945 (2002).
- ⁶²E. R. DUFRESNE, M. F. HSU, and D. A. WEITZ, *Bull. Am. Phys. Soc.* (2005).
- ⁶³J. PINERO, L. BHUIYAN, and D. BRATKO, *J. Chem. Phys.* **120**, 11941 (2004).
- ⁶⁴G. S. ROBERTS, R. SANCHEZ, R. KEMP, T. WOOD, and P. BARTLETT, *Langmuir* **24**, 6530 (2008).

- ⁶⁵S. K. SAINIS, V. GERMAIN, C. O. MEJEAN, and E. R. DUFRESNE, *Langmuir* **24**, 1160 (2008).
- ⁶⁶T. K. DE and A. MAITRA, *Advances in Colloid and Interface Science* **59**, 95 (1995).
- ⁶⁷C. MATHEW, P. K. PATANJALI, A. NABI, and A. MAITRA, *Colloids and Surfaces* **30**, 253 (1988).
- ⁶⁸G. S. GREEST, I. WEBMAN, S. A. SAFRAN, and A. L. R. BUG, *Phys. Rev. A* **33**, 2842 (1986).
- ⁶⁹J. S. HUANG, S. A. SAFRAN, M. W. KIM, G. S. GREEST, M. KOTLARCHYK, and N. QUIRKE, *Phys. Rev. Lett.* **53**, 592 (1984).
- ⁷⁰H. DIAMANT and D. ANDELMAN, *Curr. Opin. Colloid Interface Sci.* **22**, 94 (2016).
- ⁷¹H.-F. EICKE, Surfactants in nonpolar solvents, in *Micelles*, pp. 85–145, Springer, 1980.
- ⁷²B. TAMAMUSHI and N. WATANABE, *Colloid & Polym. Sci.* **258**, 174 (1980).
- ⁷³S. KISLENKO and V. RAZUMOV, *Colloid J.* **79**, 76 (2017).
- ⁷⁴P. D. FLETCHER, A. M. HOWE, and B. H. ROBINSON, *J. Chem. Soc., Fara. Trans. 1: Phys. Chem. Cond. Phases* **83**, 985 (1987).
- ⁷⁵J. MEJUTO, J. MORALES, O. MOLDES, and A. CID, *J. Appl. Solution Chem. Model.* **3**, 106 (2014).

TABLE I. Solution composition and average quantities for each aggregate, including R_g , radius of gyration, and A_s , asphericity.

N_{AOT}	10	20	30	40	50	60	70	80	90	100
N_{ISO}	3500	3500	3500	3500	3500	3500	3500	7000	7000	7000
R_g [nm]	1.04	1.17	1.31	1.47	1.58	1.67	1.79	1.78	1.97	2.07
A_s	0.48	0.18	0.21	0.16	0.18	0.11	0.20	0.22	0.18	0.10

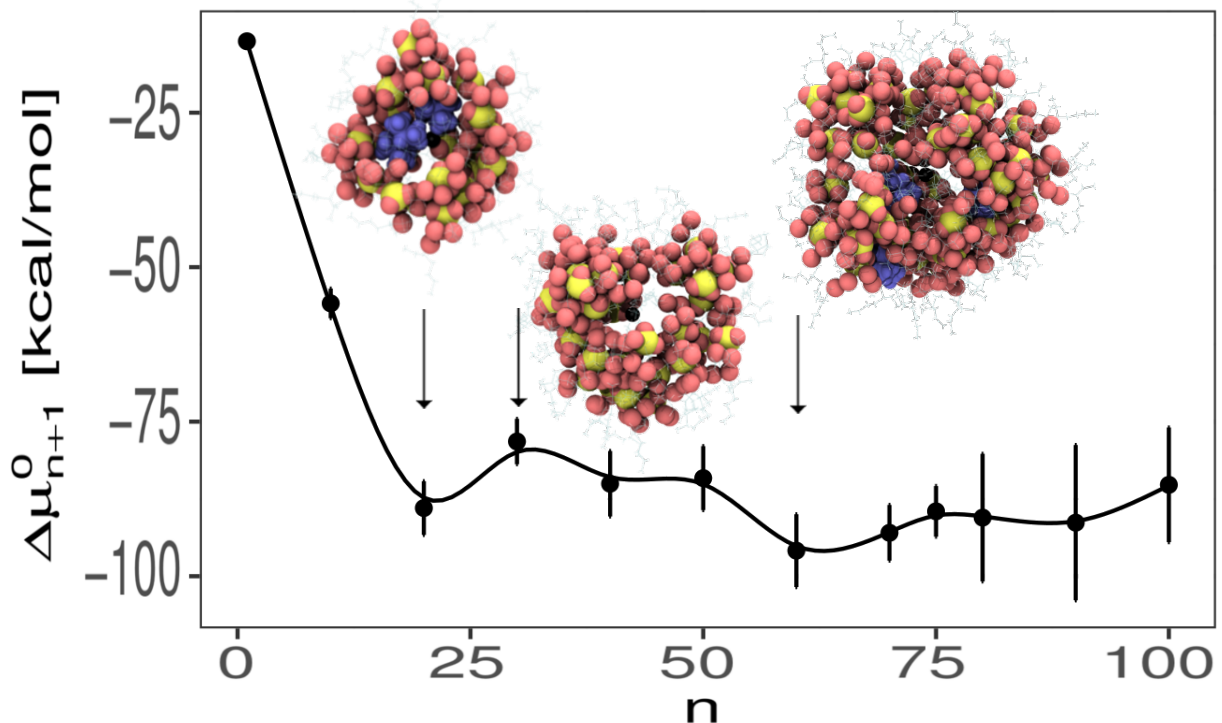


FIG. 1. The differential chemical potential, representing the change in free energy at standard state for a surfactant molecule to be added to a preexisting n aggregate, is shown as a function of n . Representative structures are shown for $n = 20$, $n = 30$ and $n = 60$. The black sphere is the center-of-mass of the aggregate. In the snapshots, the oxygen and sulfur atoms of the head group of the AOT molecule are represented by a CPK model while the aliphatic surfactant tails are represented by lines. The blue molecule in $n = 60$ is an isooctane molecule confined in the core of the “dry” AOT surfactant aggregate.

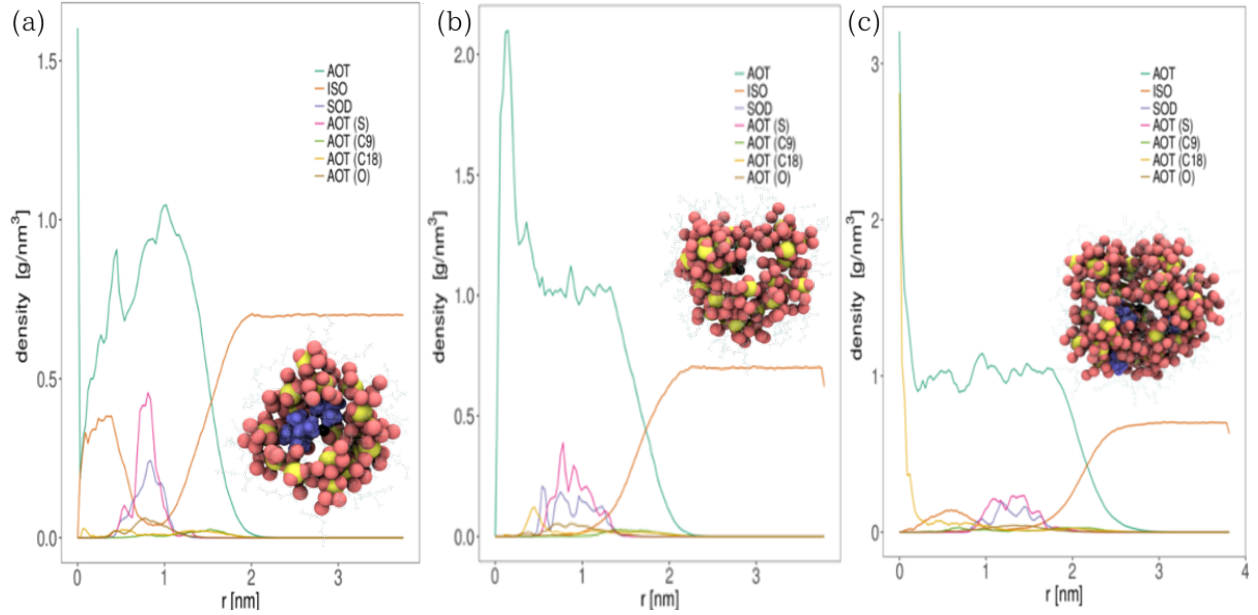


FIG. 2. The mass density of many surfactant components are depicted as a function of distance from the center-of-mass of the “dry” RM aggregate for $n =$ (a) 20, (b) 30, and (c) 60. In the snapshots, the oxygen and sulfur atoms of the head group of the AOT molecule are colored red and yellow, respectively, and the aliphatic surfactant tails are transparent gray. The isooctane molecules occupying the “dry” RM core are shown in blue.

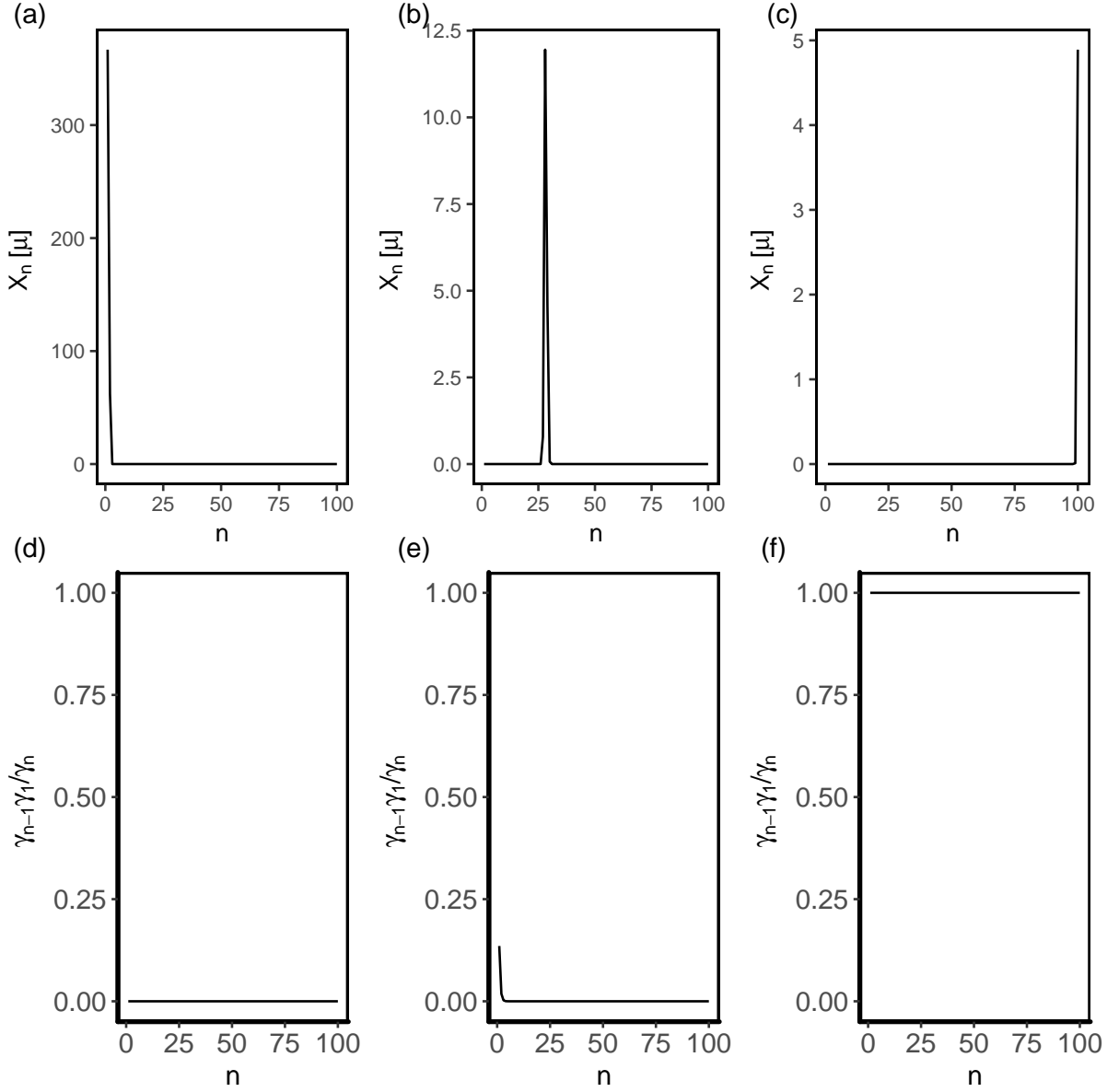


FIG. 3. The surfactant aggregate number distribution is shown for varying slope parameters ranging from (a) smallest values for the monomer state through, (b) a gradual increase, and (c) the liquid crystal state corresponding to ideal solution conditions. Shown below each plot is the corresponding activity coefficient ratio as a function of n for the corresponding size distributions in (d), (e) and (f).

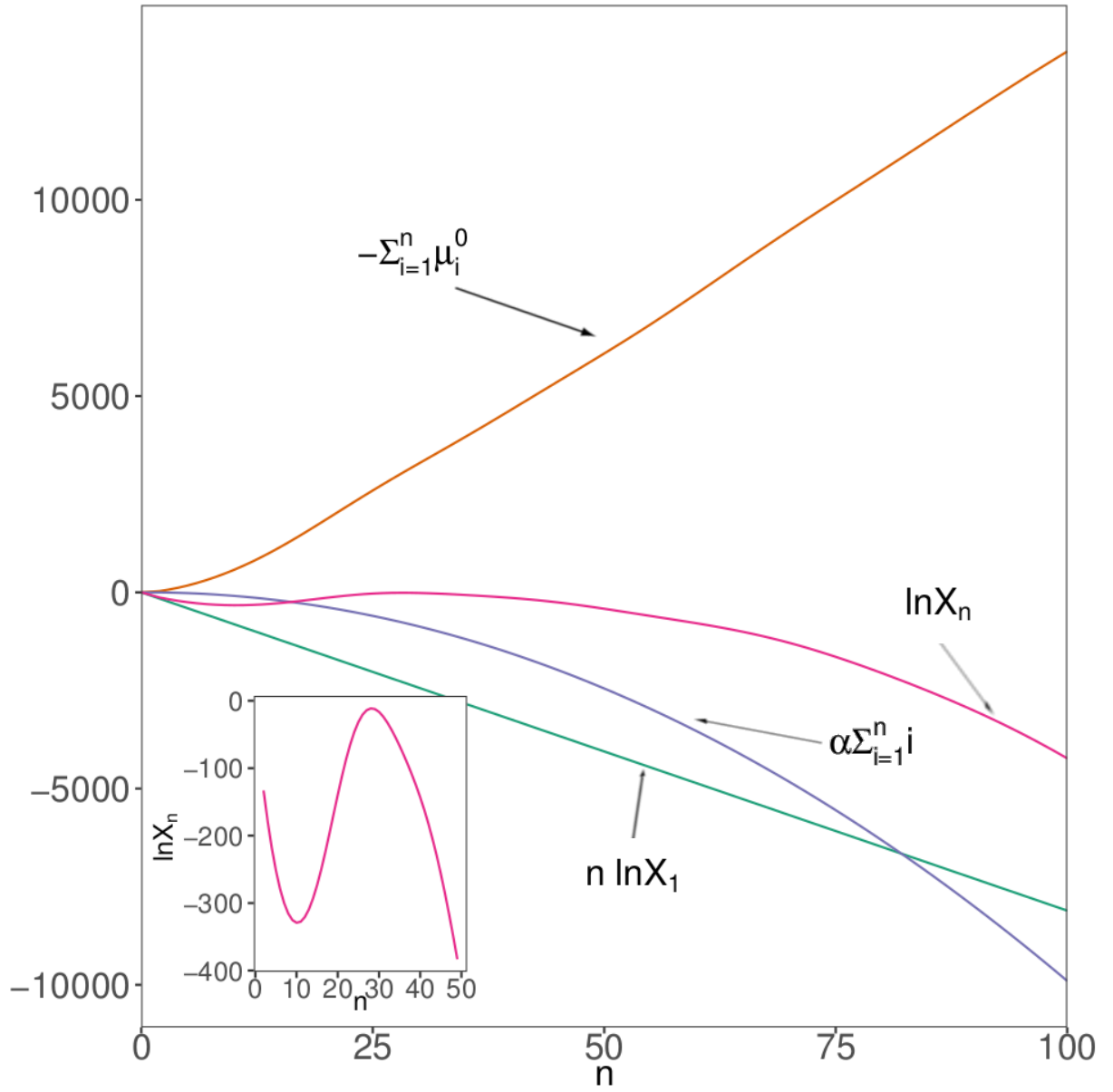


FIG. 4. Individual terms contributing to Eq. (33) as a function of aggregate size. The inset figure shows the expansion of the logarithm of the aggregate mole fraction. The slope value, α , is set to -2 . The X_1 value is set such that the total AOT concentration is the *CMC*.

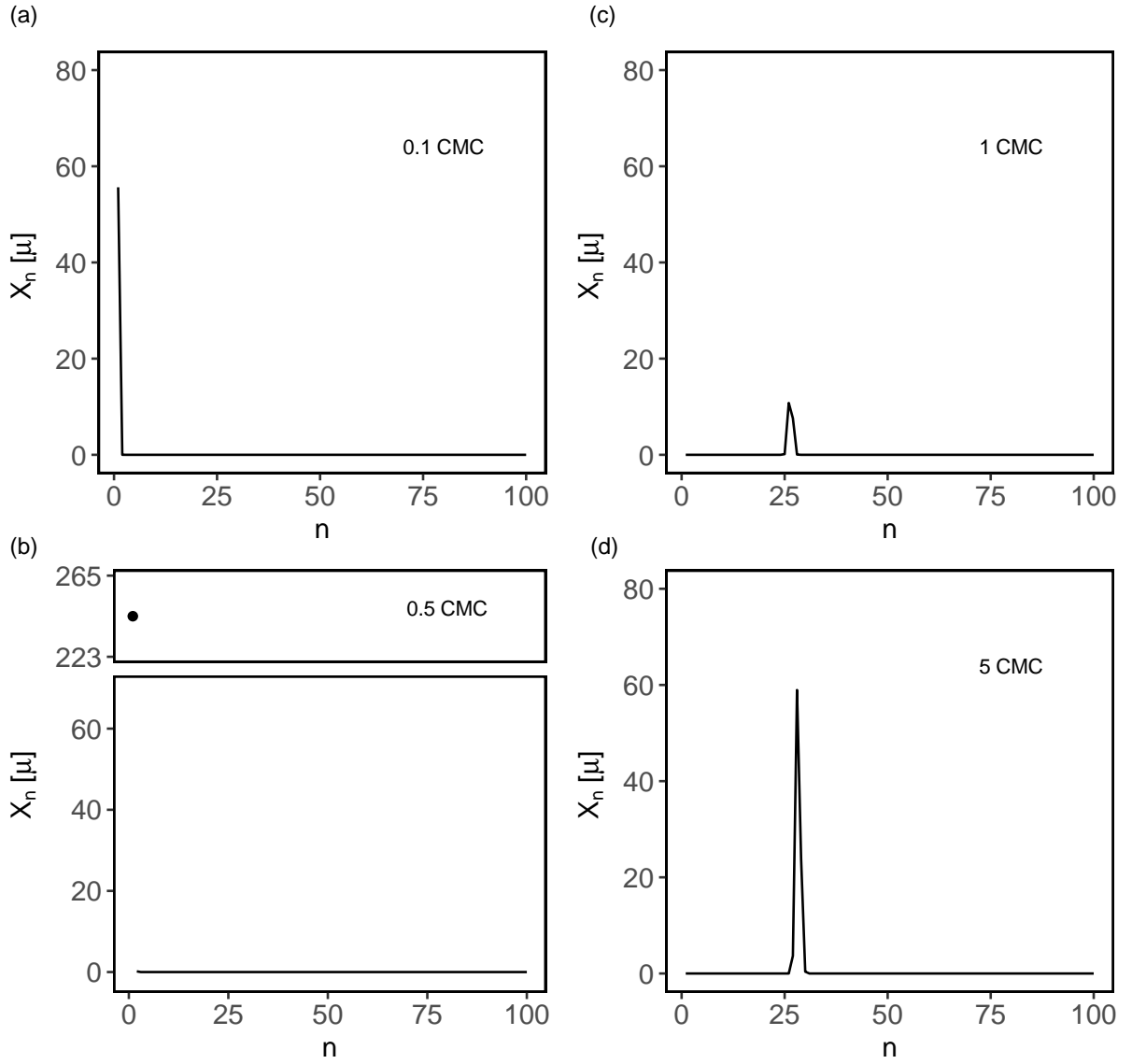


FIG. 5. The micelle size distribution is shown as a function of total concentration of AOT molecules for four values of the concentration ranging from 0.1 CMC to 5 CMC. The slope parameter α defining the size scaling of the ratio of activity coefficients was fixed to form micelles at a CMC=0.0049 M.

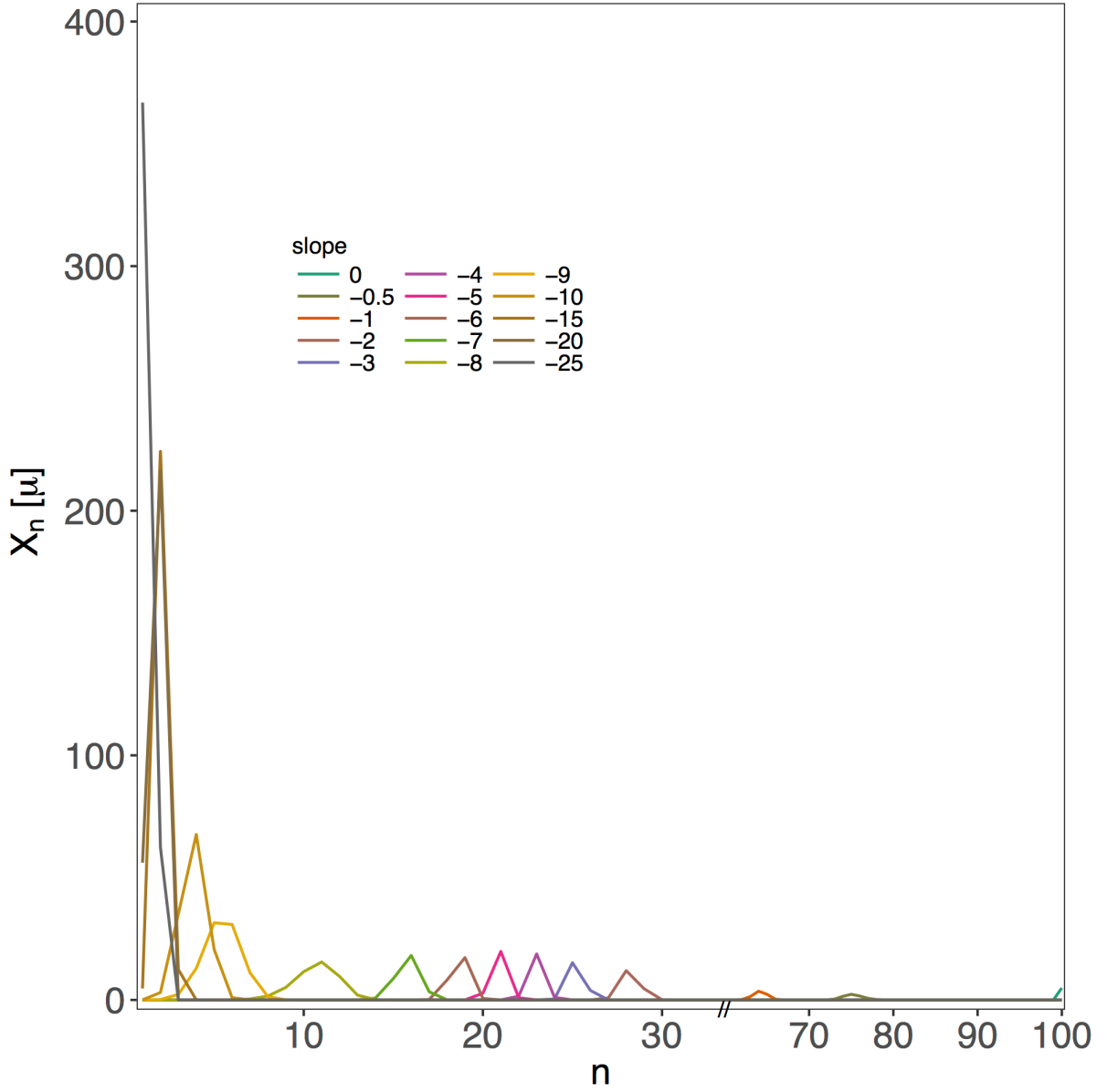


FIG. 6. The aggregate size distribution for variations in the critical *slope* parameter determining the scaling of the ratio of activity coefficients, $\log(\frac{\gamma_M \gamma_1}{\gamma_{M+1}})$. Values span a range from near activity coefficient 0 (an extreme “salt-out” condition) to 1 (an ideal solution condition). The total concentration is fixed to be the CMC.

LIST OF FIGURES

- 1 The differential chemical potential, representing the change in free energy at standard state for a surfactant molecule to be added to a preexisting n aggregate, is shown as a function of n . Representative structures are shown for $n = 20$, $n = 30$ and $n = 60$. The black sphere is the center-of-mass of the aggregate. In the snapshots, the oxygen and sulfur atoms of the head group of the AOT molecule are represented by a CPK model while the aliphatic surfactant tails are represented by lines. The blue molecule in $n = 60$ is an isooctane molecule confined in the core of the “dry” AOT surfactant aggregate. 27
- 2 The mass density of many surfactant components are depicted as a function of distance from the center-of-mass of the “dry” RM aggregate for $n =$ (a) 20, (b) 30, and (c) 60. In the snapshots, the oxygen and sulfur atoms of the head group of the AOT molecule are colored red and yellow, respectively, and the aliphatic surfactant tails are transparent gray. The isooctane molecules occupying the “dry” RM core are shown in blue. 28
- 3 The surfactant aggregate number distribution is shown for varying slope parameters ranging from (a) smallest values for the monomer state through, (b) a gradual increase, and (c) the liquid crystal state corresponding to ideal solution conditions. Shown below each plot is the corresponding activity coefficient ratio as a function of n for the corresponding size distributions in (d), (e) and (f). 29
- 4 Individual terms contributing to Eq. (33) as a function of aggregate size. The inset figure shows the expansion of the logarithm of the aggregate mole fraction. The slope value, α , is set to -2 . The X_1 value is set such that the total AOT concentration is the CMC 30
- 5 The micelle size distribution is shown as a function of total concentration of AOT molecules for four values of the concentration ranging from 0.1 CMC to 5 CMC. The slope parameter α defining the size scaling of the ratio of activity coefficients was fixed to form micelles at a $CMC=0.0049$ M. 31

6	The aggregate size distribution for variations in the critical <i>slope</i> parameter determining the scaling of the ratio of activity coefficients, $\log(\frac{\gamma_M \gamma_1}{\gamma_{M+1}})$. Values span a range from near activity coefficient 0 (an extreme “salt-out” condition) to 1 (an ideal solution condition). The total concentration is fixed to be the CMC.	32
---	---	----